

Quantum Confinement and Matrix Effects in Silver-Exchanged Soda Lime Glasses

G. Speranza,^{*,†} L. Minati,[†] A. Chiasera,[‡] M. Ferrari,[‡] G. C. Righini,[§] and G. Ischia^{||}

FBK-irst, via Sommarive 18, 38050 Povo-Trento, Italy, CSMFO Laboratory, CNR-IFN, via alla Cascata 56/C, 38050 Povo-Trento, Italy, Department of Materials and Devices, CNR, via dei Taurini 19, 00185 Roma, Italy, Optoelectronic Technologies Laboratory, Nello Carrara Institute of Applied Physics, IFAC-CNR, via Panciatici 64, I-50127 Firenze, Italy, and Materials Engineering and Industrial Technologies Department, University of Trento, via Mesiano 77, 38100 Trento, Italy

Received: November 24, 2008

This work deals with the X-ray photoelectron spectroscopy study of small silver nanoparticles embedded in soda lime glass, which is a system largely employed in integrated optics. Silver dispersions with different concentrations in the host network were obtained through ion exchange without any successive annealing. Modification of the electronic structure of Ag as well as the role of the host matrix were investigated. Experiments show that silver condensates in nanoclusters whose dimensions depend on the Ag concentration. Electronic quantum confinement related to metallic nanoparticles is observed from analyses of the core line, Auger and valence band features.

Introduction

Quantum size effects of metal nanoparticles embedded in glassy matrix have been of particular interest during the last three decades. This interest is linked to the peculiar electronic properties of metal nanoparticles, which have immediate technological implications,¹ particularly in heterogeneous catalysis,^{2–4} photonics,^{5–8} and electronics.^{9,10} Early studies on noble metal nanoparticles in glasses date back to the 1960s with the work of Doremus et al.¹¹ This pioneering work stimulated theoretical studies on metal nanoclusters and quantum confinement.^{12–14} Later, a contribution in this active area of research was given by the works of Mason,^{15,16} further supported by the studies of Wertheim and co-workers^{17,18} and very recently by Balamurugan and Maruyama.¹⁹ These authors used X-ray excitation to directly probe the electron configuration of metal nanoclusters deposited on various specific substrates such as graphite, silicon, mica, and vitreous silica. Because the process of photoemission from solids is strictly dependent on the electronic configuration of the analyzed atoms, they observed sensible modifications of the X-ray photoelectron (XP) spectral features as the size of the metallic system reduces to the nanoscale. In particular, a transition from a metallic to a semiconducting character was observed. The shape of the photoelectron core line spectra is, in fact, the result of a variety of distinct processes. Among them, extrinsic energy losses are due to scattering processes, which are characteristic of electron transport from emitting atoms to the system's surface, leading to extrinsic plasmon excitations. Intrinsic losses related to excitation of electrons in unoccupied states are present as well (*shakeup* and *shake-off* processes).²⁰ A third process influencing the photoelectron spectra is related to generation of a core photohole, which in turn produces a Coulomb-like potential. The latter causes generation of an intrinsic plasmon associated with conduction electrons in an

excited state.²¹ The metallic–nonmetallic character of the analyzed material directly influences the hole lifetime and the strength of this perturbation. Strong asymmetry of the core lines in metals associated with the presence of core-hole screening^{22,23} is described by the Doniach-Sunjić (DS) power law.²⁴ Metallic nanoparticles have a limited number of electrons in the conduction band, causing a reduction of core-hole screening.^{15–18} Moreover, when dimensions lower to the nanoscale, the system tends to assume an atomic-like behavior. This is mirrored by the narrowing of the valence bands (VB) and by the generation of an energy gap E_g . Quantum size effects are also visible on the core lines because when core-hole screening decreases, the core line loses the original DS line shape and moves to higher binding energies (BE).

Besides studies carried out to understand changes in the electronic structure induced by the reduction of particle dimensions to the nanoscale, other authors investigated the optical properties of these systems. A list of papers published in the literature deals with metal nanoparticles embedded in rare earth-activated glasses, a material of interest for telecommunication application. This research was stimulated by the need to overcome practical limitations due to (i) the small oscillator strength of the intra- $4f$ transitions of technological interest such as $^4I_{13/2} - ^4I_{15/2}$ of Er^{3+} at $1.54 \mu\text{m}$ and (ii) the quenching processes such as concentration quenching and upconversion in Er-doped glasses.^{5,7,8,25,26} The work of Malta et al.⁵ is a pioneering study on the physics underlying rare earth luminescence enhancement induced by the presence of small silver particles embedded in the matrix. Analysis of the effects of silver doping in glasses is complicated because single ions, clusters of a few atoms, and nanoparticles of various sizes can coexist.^{8,25–28} Recently, however, Martens and Polman have shown that the photoluminescence (PL) intensity of optically active erbium ions positioned in close proximity to anisotropic Ag nanoparticles is significantly enhanced if the nanoparticles support plasmon modes that are resonant with erbium emission.⁷

This large amount of data indicates that optimization of the device efficiency requires the study of the interaction of metal nanoparticles with the environment, namely, investigation of

* Corresponding author. E-mail: speranza@fbk.eu. Telephone: ++39 0461 314 487. Fax: ++39 0461 314 487.

[†] FBK-irst.

[‡] CNR-IFN.

[§] CNR and IFAC-CNR.

^{||} University of Trento.

the electronic configuration of nanoclusters embedded in the host network.

In this work, we performed XPS and TEM measurements to analyze Er^{3+} -activated soda lime glasses containing different amounts of silver in order to investigate quantum confinement of electrons in one of the most common systems used in integrated optics.²⁹ With respect to the usual fabrication protocol, which insists on control of the size of silver nanoparticles by thermal annealing of silver-exchanged glasses, we work with as-prepared samples in this paper, differing only by silver content. Different spectral regions were investigated with the aim to correlate changes of line shape and binding energies to the chemical state and size of silver particles. Further incentive for performing this study is the fact that an increase in amplitude of 1.5 μm luminescence in Ag-exchanged soda lime glasses has been demonstrated for nonresonant Er^{3+} excitation, when the excitation wavelength is in the same spectral range as the plasmon absorption of silver nanoparticles.^{8,25,26,30}

Experimental Section

Molar composition of the Er–Yb-activated glass is as follows: 67 SiO_2 , 14.4 Na_2O , 9.1 CaO , 1.9 Al_2O_3 , 0.9 P_2O_5 , 0.9 K_2O , 1.9 Er_2O_3 , and 3.9 Yb_2O_3 (mol %). Four samples were produced cutting the glasses into plates, which were thinned to 200 μm and optically polished. One plate was kept as a glass reference for absorption measurements, while three other samples were Ag^+ ion-exchanged by keeping them at 390 $^\circ\text{C}$ for 67 h in a molten salt bath of NaNO_3 , containing a variable molar concentration (0.5, 1.5, and 5%) of AgNO_3 . These ion-exchanged plates will be referred to as SAg0.5, SAg1.5, and SAg5.0, respectively.

Absorption measurements were performed using a Cary 5000 UV–vis NIR spectrophotometer in dual beam mode.

XPS measurements were taken on SAg samples as well as on a pure soda lime glass and on a pure (99.99%) silver sample (AgRef), previously sputter cleaned, which were used as references for data analysis. The XP spectra were acquired by using a Scienta ESCA 200 analyzer (Gammadata, Sweden) equipped with a monochromatized $\text{Al K}\alpha$ X-ray source. Core lines were acquired at 150 eV pass energy that corresponds to an energy resolution of 0.35 eV, taking into account the effects of charge compensation. Auger and valence band spectra were acquired at 300 eV pass energy to increase the signal-to-noise ratio without significant loss of spectral resolution. All spectra were aligned fixing the C1s deriving from contamination at 284.6 eV.³¹ We note that a nonoptimal charge compensation may contribute to spectral broadening. For this reason, to reduce the extent of charging, the X-ray source was operated at 300 W, instead of its maximum power of 500 W. The SiO_2 core line was always perfectly symmetric with a full width at half-maximum (fwhm) in the range of 1.7–1.9 eV, comparable with those reported in the literature for silicate glasses.^{32,33} During spectral acquisition, we did not observe any peak drift, therefore, confirming the homogeneity and stability of the compensation.

Oxygen core line peak fitting was performed using three Gaussian components. Each of them is associated with a specific chemical bond formed by oxygen with other chemical elements in the soda lime glass. Four components were needed to fit the Ag 3d doublets to describe the oxidized and nonoxidized states of silver in the glassy matrix. Voigt line shape was employed to fit the Ag 3d reference spectra. The Auger parameter was computed fitting the $\text{M}_4\text{N}_{45}\text{N}_{45}$ spectra with five Gaussian components. The number and energy positions of these components were selected on the basis of the shape of the Auger

TABLE 1: Binding Energy (BE) and Integrated Intensity (I) of Two Ag 3d_{5/2} Gaussian Components, Ag 3d_{5/2} Peak fwhm, Auger Parameter (α), Fermi Cutoff Energy, and Valence Band Width (VB_w)

samples	Ag 3d BE (eV)	Ag 3d I (%)	Ag 3d fwhm (eV)	α (eV)	Fermi cutoff (eV)	VB _w (eV)
AgRef	368.22	—	0.5	726.0	0	2.0
SAg0.5	368.48	20.2	1.5	724.8	0.8	1.4
	367.68	79.8				
SAg1.5	368.59	66.4	1.6	725	1.4	1.5
	367.77	33.5				
SAg5.0	368.50	83.9	1.3	725.3	1.7	1.8
	367.70	16.1				

spectrum from the pure Ag sample (AgRef), where the structures are well-defined. After background subtraction, the position of the Fermi cutoff was estimated by fitting the step spectra with a linear function and taking the midpoint position on the stepping shoulder as the value for the Fermi cutoff. To study Ag VB, subtraction of the pure glass contribution was performed after normalization of the spectra to oxygen 2p integrated intensities. The remaining Ag 4d band was fitted using two Gaussian components. Maintaining their width unchanged, the Gaussian positions allowed us to describe changes in the VB width (VB_w) due to changes in the Ag cluster dimension.

We also prepared specimens for TEM observations by scraping off thin films in absolute ethanol using a diamond knife. A drop of the suspension was deposited and dried onto a carbon-coated copper grid. Samples were observed using a Philips CM12 TEM operated at 120 kV and equipped with an energy dispersive X-ray spectrometer (EDXS).

Results

Three series of measurements were performed on samples SAg0.5, SAg1.5, and SAg5.0. Table 1 reports average values obtained from the XP spectra.

Figure 1 shows the absorption spectra of the SAg samples. The sharp weak peaks are due to Er^{3+} and Yb^{3+} absorption.²⁹ The intense band centered at 443 nm in the absorption spectrum of the SAg5.0 plate arises from surface plasmon absorption of Ag nanoparticles.^{14,19,25}

Figure 2 shows the XPS Ag 3d core level spectra for the ion-exchanged soda lime glasses and for the bulk silver reference. Doublet structures corresponding to 3d_{5/2} and 3d_{3/2} electrons are due to spin–orbit splitting. The BE of the Ag core line increases with Ag concentration in the glasses. In Table 1, the position and relative integrated intensities are reported for

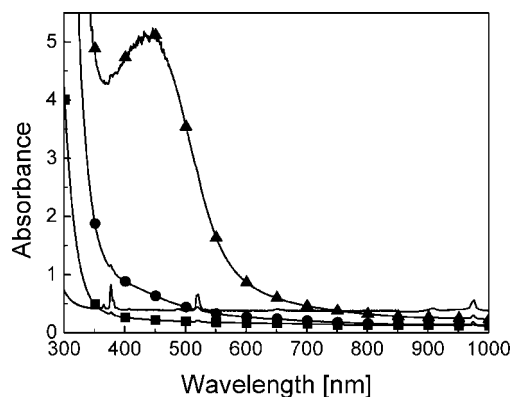


Figure 1. Absorption spectra of ion-exchanged soda lime glasses as a function of silver content. Solid line, nonexchanged glass (10 times magnified); squares, SAg0.5; circles, SAg1.5; and triangles, SAg5.0.

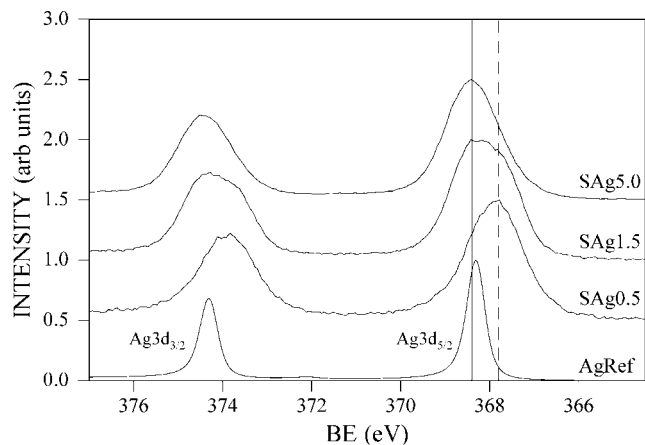


Figure 2. XPS Ag 3d core level spectra for the ion-exchanged soda lime glasses (SAG) and for the bulk silver reference (AgRef). The spin-orbit components, $3d_{5/2}$ and $3d_{3/2}$, are labeled. Solid and broken lines indicate the BE of Ag nanoclusters and silver oxide, respectively.

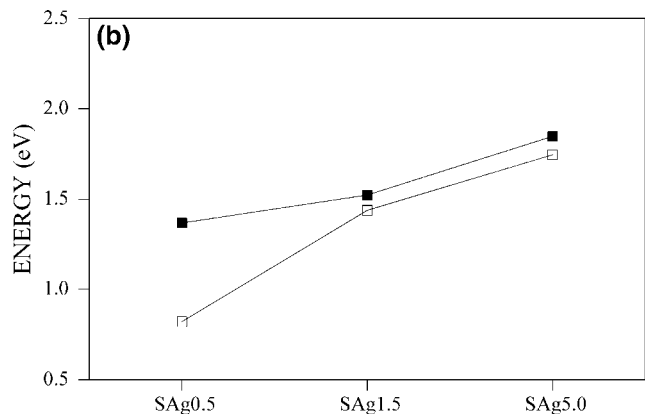
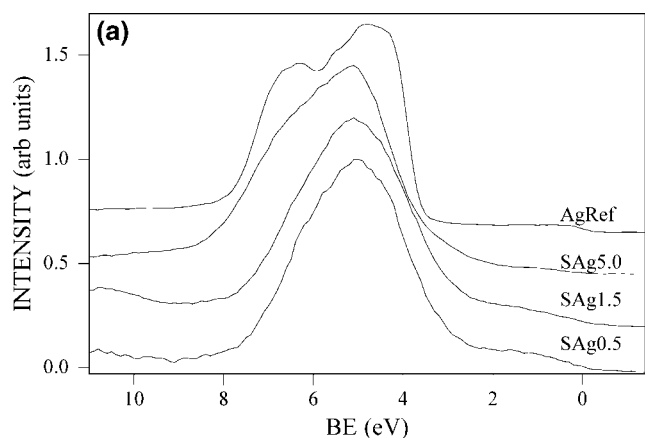


Figure 3. (a) XPS valence band of the SAG and AgRef samples upon subtraction of the pure soda lime VB contribution. (b) Position of the Fermi cutoff (\square) and values of the VB width (VB_w) for the SAG ion-exchanged samples (\blacksquare). The solid line is a guide for the eyes.

the two Gaussian components used to fit the Ag $3d_{5/2}$ peak as well as its fwhm.

Figure 3a shows the XPS valence band of the SAG and AgRef samples upon subtraction of the pure soda lime VB contribution. It is apparent that the VB undergoes a loss of feature definition. VB width (VB_w) of the ion-exchanged glasses (Table 1) increases with increasing Ag content but remains smaller than that of the silver reference. Figure 3b shows the position of the Fermi cutoff and the VB_w for the SAG ion-exchanged samples; the higher the VB_w , the higher the amplitude of the gap at the

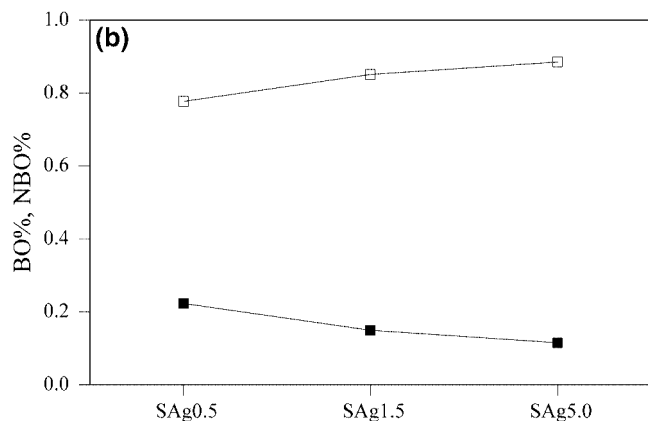
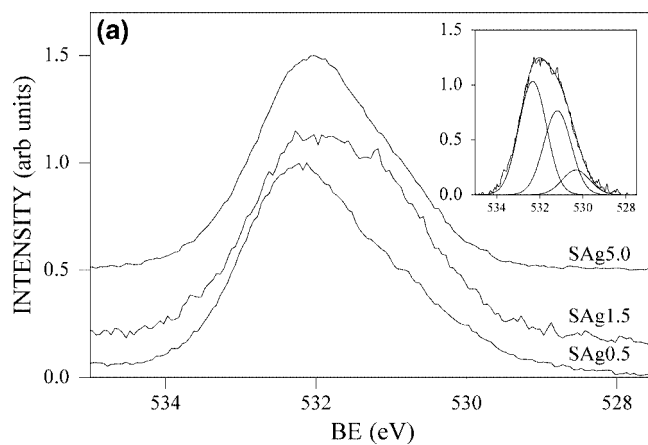


Figure 4. (a) Evolution of the oxygen core line as a function of silver content. The inset shows an example of peak fitting performed on the oxygen core line (sample SAg1.5), using three Gaussian components. (b) Relative amount of bridging oxygens (\square) and nonbridging oxygens (\blacksquare) for the SAG ion-exchanged samples. The solid line is a guide for the eyes.

TABLE 2: Relative Amount of BO and NBO in SAG samples: $\text{BO}\% = \text{BO}/(\text{BO} + \text{NBO})$ and $\text{NBO}\% = \text{NBO}/(\text{BO} + \text{NBO})$

samples	BO%	NBO%
SAg0.5	78	22
SAg1.5	85	15
SAg5.0	88	12

Fermi edge. Also, the silver $\text{M}_4\text{N}_{45}\text{N}_{45}$ Auger spectra were acquired to compute modified Auger parameters, α , which are reported in Table 1.

Finally, to complete the survey, Figure 4a shows the evolution of the oxygen 1s ($\text{O}1s$) core line as a function of Ag content. The inset shows the decomposition of three Gaussian components for sample SAg1.5. The component at 532.3 eV is related to the bridging oxygen (BO) in SiO_2 ; the component at 530.3 eV is assigned to the nonbridging oxygen (NBO) atoms, and the component at 531.2 eV is due to other oxides present in the glass.^{34,32} Similar binding energy values were obtained for the other SAG samples. The relative amount of BO and NBO was obtained by the integrated intensity of the corresponding Gaussian components. Figure 4b and Table 2 show the ratio of $\text{BO}\% = \text{BO}/(\text{BO} + \text{NBO})$ and $\text{NBO}\% = \text{NBO}/(\text{BO} + \text{NBO})$. Measurements show the $\text{BO}\%$ content increasing as the Ag content increases.

TEM analysis was performed on all SAG samples. Good results were obtained only from the SAg5.0-exchanged glass

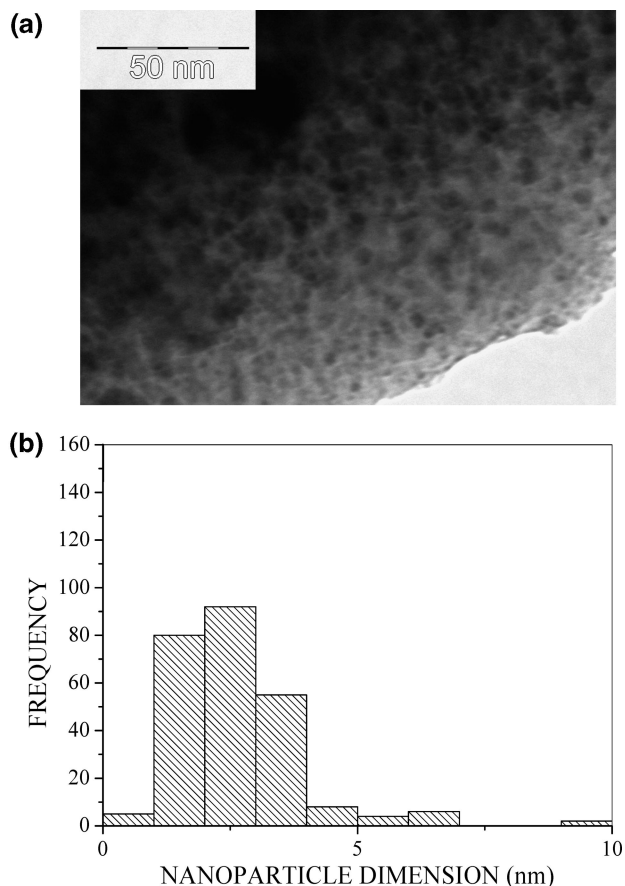


Figure 5. (a) TEM image of the SAg5.0 sample. A large quantity of small nanoparticles is visible in the lighter region of the glassy matrix. (b) Size distribution obtained from the TEM image (a).

because of its higher silver concentration. Figure 5a shows a TEM image of the SAg5.0 sample; a large amount of small nanoclusters is visible, especially in the lighter region of the photograph. Figure 5b illustrates the distribution of nanocluster dimensions, as computed from the TEM image.

Discussion

The presence of a glassy network surrounding metal nanoparticles introduces experimental and analytical complications related to the ability to (i) optimally compensate the charge in order to detect small BE shifts and (ii) single out the interactions of silver in a complex system as its concentration changes.

As seen in Figure 2 and Table 1, it is noted that with increasing silver concentration in the samples, the Ag 3d_{5/2} peak moves from lower to higher BE values, with respect to that of AgRef.

To explain this finding, at least three mechanisms may be considered: (i) the presence of surface states in competition with bulk states, (ii) the quantum confinement and reduced core-hole screening in the final state, and (iii) the role of the environment.

According to mechanism (i), the BE should approach that of the surface atoms when the cluster size become small. For metals having more than half-filled d bands, as in the case of Ag, the surface states fall to lower BE values than those found for the bulk. The transition to the nanometer size further increases this negative BE shift. However, this negative BE shift is expected to be very small in comparison to that measured for SAg0.5.¹⁸ Mechanism (ii), with reducing the cluster dimension, determines the electronic confinement and the cluster charge mobility

decrease, leading to an increase of the core-hole lifetime. In other words, there is a net reduction of core-hole screening with respect to the Ag bulk system, resulting in positive BE shifts. On the other hand, during the ion exchange process, Ag⁺ ions replace Na⁺ ions, and strong electrostatic interactions between Ag and its environment are expected. Because of this, it is also reasonable to take into account mechanism (iii).

The mechanisms presented are effective with different weights because of the complex structure of the ion-exchanged glasses. To explain the positive and negative BE shift of the Ag 3d core line, we consider that silver arranges differently in the host network on the basis of its concentration. In particular, Table 1 reports the positions and integrated intensities of two Gaussian components obtained by fitting the Ag 3d_{5/2} peak of Figure 2. For the SAg0.5 sample, the main contribution arises from the lowest-energy component. Moving from the SAg0.5 to SAg5.0 samples, the integrated intensities of the highest-energy component become predominant. In samples SAg0.5, where the Ag content is very low, Ag 3d falls at BE values close to those reported in the literature for Ag₂O at 367.9 eV and for AgO at 367.6 eV.^{35,36} This allows us to assign the lowest-energy component to oxidized silver. Besides, in insulating materials as our glasses, possible participation of charges coming from environmental ligands to the screening process was proposed in the literature.³⁷ Because the charge mobility is very low in all analyzed glassy systems, this process induces only small differences in the Ag BE of the three SAg samples. We then expect that the chemical bond with oxygen is predominant, which explains the negative BE shift with respect to AgRef. The predominance of oxidized silver with respect to silver nanoclusters is the reason for the absence of the plasmon band in the absorption spectrum of the SAg0.5 sample (Figure 1).

At higher silver concentrations, as in sample SAg5.0, a higher binding energy value with respect to the bulk is found. Now, comparing the position of the AgRef core line with that of the Gaussian component at high BE, we observed a small but significant BE positive shift of about 0.3 eV (Table 1). In agreement with the literature, we can assign the latter shift to silver nanoclusters.^{38,39} The high silver concentration causes Ag condensation into the nanoparticles, and the chemical effect becomes marginal. It is possible to estimate the mean cluster size from data in the literature.^{38,39} From these data, a BE shift of ~0.3 eV may be related to a mean cluster diameter of ~2 nm. Moreover, we observe that the Ag⁰ component of the Ag 3d core line was fitted with a Gaussian component, indicating the size distribution is sharp,⁴³ and the quantum confinement is responsible for line broadening.

These results are confirmed by the intense absorption band of the SAg5.0 slab due to the surface plasmon of silver nanoclusters (Figure 1) and by TEM analysis (Figure 5a,b). The average diameter, *d*, of the silver nanoclusters can also be calculated from the fwhm of the optical absorption peak, using the relation

$$d = \frac{\nu_f \lambda_p^2}{\pi c \Delta\lambda}$$

where ν_f (1.39×10^8 cm s⁻¹) is the Fermi velocity of electrons in bulk silver, *c* is the speed of light, and λ_p and $\Delta\lambda$ are the characteristic wavelength and the fwhm of the surface plasmon resonance, respectively.⁴⁰⁻⁴² Using $\lambda_p = 443$ nm and fwhm ~ 150 nm obtained from the absorption spectrum of Figure 1, we roughly estimate an average diameter of about 2 nm for the SAg5.0 sample, which is in agreement with that obtained from XPS analysis.

A very good agreement was also obtained when comparing the XPS analysis with TEM images. Figure 5a shows that the SAg5.0 glassy matrix is populated with a high number of silver nanoparticles. The size distribution, estimated on a population of 260 TEM spots, appears to be rather sharp and centered at ~ 2.5 nm, as shown in Figure 5b. TEM analyses were also performed on SAg1.5 and SAg0.5 samples. A lower Ag content, the presence of a high abundance of silver oxide, and the high mobility of silver in the soda lime glass prevented the acquisition of TEM images suitable to measure the nanoparticle dimension. On the other hand, higher silver concentrations should correspond to larger nanoparticles. We then expect that an average nanocluster dimension of ~ 2 nm is also a good estimate for the SAg1.5 sample.

With respect to this latter sample, an intermediate situation occurs, where the absorption is still present but to a lesser extent (Figure 1). The chemical and structural states described for samples SAg0.5 and SAg5.0 are now simultaneously visible. As seen in Figure 2 and Table 1, the fwhm of the Ag 3d peak is higher than those of samples SAg0.5 and SAg5.0. This broadening corresponds to high intensities for the two Gaussian components related to silver oxide and silver nanoparticles. Also the position of the Ag⁰ component falls at a slightly higher BE, which corresponds to a mean diameter of ~ 1.8 nm.

All of these results are consistent with the values calculated for Auger parameter, α , reported in Table 1. The α value of 724.8 eV measured for SAg0.5 is very close to the value of 724.5 eV reported in refs 35 and 36 for silver oxide. A slightly larger value of α is found for samples SAg1.5 and SAg5.0, which falls between those of silver oxide and pure bulk silver. Although, in the case of silver, the influence of quantum confinement on the Auger parameter is very small, a decrease with respect to the pure metal is expected with the presence of the initial and final state effects.⁴⁴

This interpretation also agrees with the position of the Fermi cutoff and with values of VB_w. Referring to the values of the Fermi cutoff presented in Table 1, we can see in the presence of silver oxide (sample SAg0.5) the Fermi cutoff is placed at 0.8 eV, which is in good agreement with the literature.^{45–47} In sample SAg1.5, because of the coupled effect of electron quantum confinement³⁸ and of the presence of oxide, the Fermi cutoff moves to 1.4 eV (Table 1). Finally, in sample SAg5.0, quantum confinement dominates over the influence of oxide, giving a higher BE for the Fermi cutoff of 1.8 eV (Table 1 and Figure 3b). This trend is consistent with results obtained by Wertheim,³⁸ although the presence of the glassy environment in our case leads to different values of Fermi cutoff positions. With respect to the trend of VB_w summarized in Table 1, all VB_w values for the three samples are lower than that of pure bulk silver because of strong electron localization. The VB_w value relative to sample SAg0.5 reflects the presence of highly localized electron states due to bonds with oxygen. An intermediate situation is found for sample SAg1.5, where the value of VB_w slightly increases. Finally, for sample SAg5.0, where the quantum confinement is dominant, the VB acquires a more relevant metallic character, and the VB_w value comes close to the value measured for AgRef. The effect of quantum confinement leads to a 4d bands narrowing,³⁸ which is limited by the presence of a cluster size distribution, especially for the SAg5.0 sample.

The effect of the glassy matrix and involvement of silver valence electrons in chemical bonds are also explained by analyzing the oxygen core line (Figure 4a). The interaction of silver with oxygen in the glassy matrix must determine chemical

shifts. Further, Ag clustering leads to unpaired oxygen atoms in the host matrix and to silver aggregates not well-coordinated to oxygen. The oxygen core line was deconvoluted in three Gaussian components, as shown in the inset of Figure 4a. As is shown in Figure 4b, the BO% increases with increasing silver concentration in SAg samples. The insertion of Ag in the samples leads to strong modification of the glassy network. The trend of BO%, NBO%, and the silver behavior can be described with the following structural model. At low Ag concentrations, silver atoms replace sodium atoms, and a strong interaction with oxygen atoms takes place. This is the case with a higher NBO% value. With an increase in silver concentration, unpaired oxygen radicals and Ag⁰ atoms formed. The high Ag⁰ mobility leads to the formation of Ag clusters with the oxygen radicals free to rearrange with silicon. This induces a silica network reconstruction with the emission of oxygen atoms in excess.³¹ The increase of BO% with increasing amounts of silver, shown in Figure 4b and Table 2, confirms this model. Also, the small shift of the Si 2p BE core lines to higher BE (not reported here) describes the change in the chemical state of this element associated with this chemical process.³⁴

Conclusions

X-ray photoelectron spectroscopy was performed on three Ag-exchanged soda lime glasses produced for photonic applications. The aim of this work was to understand the effect of different Ag concentrations on the electronic structure of silver nanoparticles in the glassy network. Different spectral features were analyzed to clarify the effect of progressive silver clustering. Our results are listed:

- A strong interaction between oxygen of the glassy matrix and silver is present, as shown by the trend of BO% and NBO%.
- At lowest concentrations, Ag is mainly in oxidized form and nanoclusters constitute a minor part of the total amount of silver exchanged.
- At intermediate concentrations, both silver nanoparticles and silver oxides are present, leading to marked changes of the spectral features such as fwhm of Ag 3d_{5/2}, Fermi cutoff position, and value of the Auger parameter.
- At higher Ag concentration, silver is essentially condensed in nanoparticles consistent with the higher BE of the Ag 3d core lines, Fermi cutoff positions, and values of the relative Auger parameter.
- The VB_w value reflects an increasing metallic character, when increasing the Ag content of the samples.

These results confirm that XP spectral changes correspond to well-defined chemical and structural organization of silver in the soda lime glasses. In particular, the position of the Ag 3d core line at the intermediate and higher silver concentrations corresponds to clusters with an average diameter of about 2 nm. Gaussian fit suggests that quantum confinement effects are predominant in Ag⁰ 3d_{5/2} line broadening. These results are in agreement with the estimates obtained from the plasmon resonance frequency and TEM analysis.

The obtained results enrich the knowledge of the structure and physical phenomena that are involved in the performance of glasses with potential photonic applications.

Acknowledgment. This research was performed in the framework of COST Action MP0702.

References and Notes

- (1) Sun, Y.; Xia, Y. *Science* **2002**, 298, 2176.
- (2) Somorjai, G. A.; Rioux, R. M. *Catal. Today* **2005**, 100, 201.

- (3) Trong-On, D. *Recent Res. Dev. Chem.* **2004**, *2*, 29.
- (4) Meurig, T. J.; Pratibha, G. L. *Adv. Catal.* **2004**, *48*, 171.
- (5) Malta, O. L.; Santa-Cruz, P. A.; De Sa, G. F.; Azuel, F. *J. Lumin.* **1985B**, *33*, 261.
- (6) Trave, E.; Mattei, G.; Mazzoldi, P.; Pellegrini, G.; Scian, C.; Maurizio, C.; Battaglin, G. *Appl. Phys. Lett.* **2006**, *89*, 151121.
- (7) Mertens, H.; Polman, A. *Appl. Phys. Lett.* **2006**, *89*, 211107.
- (8) Mattarelli, M.; Montagna, M.; Vishnubhatla, K.; Chiasera, A.; Ferrari, M.; Righini, G. C. *Phys. Rev. B* **2007**, *75*, 125102.
- (9) Moriarty, P. *Rep. Prog. Phys.* **2001**, *64*, 297.
- (10) Kershaw, S. V.; Harrison, M. T.; Burt, M. G. *Philos. Trans. R. Soc. London* **2003**, *361A*, 331.
- (11) Doremus, R. H. *J. Chem. Phys.* **1965**, *42*, 414.
- (12) Kreibig, U.; Von Fragstein, C. *Z. Phys.* **1969**, *224*, 307.
- (13) Kreibig, U. *Z. Phys.* **1970**, *234*, 307.
- (14) Kreibig, U.; Vollmer, M. *Optical Properties of Metal Clusters*; Springer: Berlin, 1995.
- (15) Mason, M. G.; Baetzold, R. C. *J. Chem. Phys.* **1975**, *64*, 271.
- (16) Mason, M. G. *Phys. Rev. B* **1983**, *27*, 748.
- (17) Wertheim, G. K.; di Cenzo, S. B.; Youngquist, S. E. *Phys. Rev. Lett.* **1983**, *51*, 2310.
- (18) Citrin, P. H.; Wertheim, G. K. *Phys. Rev. B* **1983**, *27*, 3176.
- (19) Balamurugan, B.; Maruyama, T. *J. Appl. Phys.* **2007**, *102*, 034306.
- (20) Moslemzadeh, N.; Beamson, G.; Tsakiroopoulos, P.; Watts, J. F. *Surf. Sci.* **2006**, *600*, 265.
- (21) Dow, J. D.; Flynn, C. P. *J. Phys. (Paris)* **1980**, *C13*, 1341.
- (22) Nozieres, P.; Dominicus, C. T. *Phys. Rev.* **1969**, *178*, 1097.
- (23) Wertheim, G. K. *Phys. Rev. B* **1982**, *25*, 1987.
- (24) Doniach, S.; Sunjic, M. *J. Phys. (Paris)* **1970**, *C3*, 285.
- (25) Portales, H.; Mattarelli, M.; Montagna, M.; Chiasera, A.; Ferrari, M.; Martucci, A.; Mazzoldi, P.; Pelli, S.; Righini, G. C. *J. Non-Cryst. Solids* **2005**, *351*, 1738.
- (26) Speranza, G.; Bhaktha, S. N.; Chiappini, A.; Chiasera, A.; Ferrari, M.; Goyes, C.; Jestin, Y.; Mattarelli, M.; Minati, L.; Montagna, M.; Nunzi Conti, G.; Pelli, S.; Righini, G. C.; Tosello, C.; Vishnubhatla, K. C. *J. Opt. A: Pure Appl. Opt.* **2006**, *8*, S450.
- (27) Strohhofer, C.; Polman, A. *Appl. Phys. Lett.* **2002**, *81*, 1414.
- (28) Martucci, A.; de Nuntis, M.; Ribaldo, A.; Guglielmi, M.; Padovani, S.; Enrichi, F.; Mattei, G.; Mazzoldi, P.; Sada, C.; Trave, E.; Battaglin, G.; Gonella, F.; Borsella, E.; Falconieri, M.; Patrini, M.; Fick, J. *Appl. Phys. A* **2004**, *80*, 557.
- (29) Nunzi Conti, G.; Peyghambarian, N.; Ferrari, M.; Montagna, M.; Righini, G. C.; Brenci, M.; Forastiere, M. A.; Pelli, S.; Ricci, G. *Philos. Mag.* **2002**, *B82*, 721.
- (30) Chiasera, A.; Ferrari, M.; Mattarelli, M.; Montagna, M.; Pelli, S.; Portales, H.; Zheng, J.; Righini, G. C. *Opt. Mater.* **2005**, *27*, 1743.
- (31) Wang, P. W. *Appl. Surf. Sci.* **1997**, *120*, 291.
- (32) Roy, B.; Jain, H.; Roy, S.; Chakravorty, D. *J. Non-Cryst. Solids* **1997**, *222*, 102.
- (33) Yano, T.; Azegami, K.; Shibata, S.; Masayuki, Y. *J. Non-Cryst. Solids* **1997**, *222*, 94.
- (34) Wang, P. W. *J. Vac. Sci. Technol. A* **1996**, *14*, 465.
- (35) Gangopadhyay, P.; Kesavamoorthy, R.; Santanu, B.; Magudapathy, P.; Nair, K. G. M.; Panigrahi, B. K.; Narasimhan, S. V. *Phys. Rev. Lett.* **2005**, *94*, 047403.
- (36) *NIST X-ray Photoelectron Spectroscopy Database*, version 3.4; NIST Standard Reference Database 20; National Institute of Standards and Technology: Gaithersburg, MD, 2003, <http://srdata.nist.gov/xps/>.
- (37) Veal, B. W.; Paulikas, A. P. *Phys. Rev. B* **1985**, *31*, 5399.
- (38) Wertheim, G. K.; DiCenzo, S. B.; Buchanan, D. N. E. *Phys. Rev. B* **1986**, *33*, 5384.
- (39) Wertheim, G. K.; DiCenzo, S. B. *Phys. Rev. B* **1988**, *37*, 844.
- (40) Arnold, G. W. *J. Appl. Phys.* **1975**, *46*, 4466.
- (41) Manikandan, D.; Mohan, S.; Magudapathy, P.; Nair, K. G. M. *Phys. B* **2003**, *325*, 86.
- (42) Bahniwal, S.; Sharma, A.; Aggarwal, S.; Deshpande, S. K. *J. Appl. Phys.* **2008**, *104*, 064318.
- (43) Minati, L.; Speranza, G.; Calliari, L.; Micheli, V.; Baranov, A.; Fanchenko, S. *J. Phys. Chem. A* **2008**, *112*, 7856.
- (44) Wertheim, G. K. *Phys. Rev. B* **1987**, *36*, 9559.
- (45) Tjeng, L. H.; Meinders, M. B.; van Elp, J.; Ghijsen, J.; Sawatzky, G. A. *Phys. Rev. B* **1990**, *41*, 3190.
- (46) Boronin, A. I.; Koscheev, S. V.; Zhidomirov, G. M. *J. Electron. Spectrosc. Relat. Phenom.* **1998**, *96*, 43.
- (47) Bielman, M.; Schwaller, P.; Ruffieux, P.; Groning, O.; Schlapbach, L.; Groning, P. *Phys. Rev. B* **2002**, *65*, 235431.

JP810317Q